crystals

MDPI

Article

Influence of X Cation Covalence in the Formation of Ni-O-X Mixed Oxides by Reactive Ion Beam Mixing of Ni/X Interfaces

Antonio Arranz * and Carlos Palacio

Departamento de Física Aplicada, Facultad de Ciencias, Módulo 12. Universidad Autónoma de Madrid, Cantoblanco, 28049 Madrid, Spain

* Correspondence: antonio.arranz@uam.es

Abstract: The reaction of the Ni/X interfaces (X = Si or Cr) with O_2^+ ions at low energy (3 keV) was studied using X-ray photoelectron spectroscopy (XPS) and factor analysis (FA). It was found that low ion doses lead to the formation of a NiO thin film on the surface that was progressively transformed into a Ni-O-X mixed oxide with increasing the ion dose. The degree of transformation of NiO into Ni-O-X depended on the covalence of the X cation, indicating that the reaction was influenced by chemical driving forces. For strong covalent cations (Si and Al), NiO was completely transformed into Ni-O-X at ion doses above 1.8×10^{17} ions/cm^2, whereas for ionic cations (Cr) the transformation was incomplete. The ionicity of Ni atoms in the Ni-O-X mixed oxide increased with the increase in the covalence of X cation, and the features of the Ni 2p core level, characteristic of bulk NiO which were attributed to non-local screening, disappeared.

Keywords: metal oxides; thin films; synthesis; characterization; reactive ion beam mixing; photoelectron spectroscopy

Citation: Arranz, A.; Palacio, C. Influence of X Cation Covalence in the Formation of Ni-O-X Mixed Oxides by Reactive Ion Beam Mixing of Ni/X Interfaces. *Crystals* **2023**, *13*, 345. https://doi.org/10.3390/cryst13020345

Academic Editor: Sharadrao Anandarao Vanalakar

Received: 22 December 2022
Revised: 6 February 2023
Accepted: 16 February 2023
Published: 17 February 2023

1. Introduction

In recent years, there has been an increasing demand of noble metals-free catalysts based in earth-abundant raw materials. In this way, Ni-based mixed oxides are being tested as promising candidates for substituting noble metal-based catalysts [1–19]. Ni-Co mixed oxides have been proposed for the catalytic oxidation of benzene [1] and their ability in O_2 activation during benzyl alcohol oxidation in air has also been addressed [2]. Ni-Cu mixed oxides have been tested for the catalytic hydrogen [3,4] and oxygen [4] evolution reactions. In addition, their catalytic activity for CO oxidation [5] and conversion of lignin in subcritical methanol [6] have been also studied. Ni-Al mixed oxides have been proposed for the catalytic oxidative dehydrogenation of ethane to ethylene [7] and as catalytic precursors in the hydrogenation process [8]. Ni-Mg mixed oxides catalysts have been used for low temperature methane oxidation [9] and Ni-Mg-Al mixed oxides catalysts have been tested for CO_2 methanation [10]. Likewise, Ni-Zr [11], Ni-Fe [12] and NiO/Mn-doped $NiCo_2O_4$ [13] mixed oxides have been tested as catalysts for the oxygen evolution reaction [11,12], and Ni-Mn mixed oxides for ethanol oxidation [14]. Ni-In mixed oxides have been studied in the electroreduction of CO_2 [15], and Ni-Ce mixed oxides for the catalytic CO methanation reaction [16]. Likewise, Ni-Ge mixed oxides have been tested for the electrochemical nitrogen reduction reaction [17] and Ni-Sn mixed oxides as catalysts for carbonylation of amines by CO_2. On the other hand, nickel silicates supported on olivine have been addressed for tar removal from biomass gasification [19]. Other fields of active Ni-based mixed oxides research were related to their magnetic [20] and gas-sensing properties [21].

In the above-mentioned works [1–21], a great variety of physical and chemical methods to grow Ni-based mixed oxides have been reported. In a previous work, the reactive ion beam mixing (IBM) of Ni/Al interfaces using low energy O_2^+ ions has been explored and the formation of Ni-Al mixed oxide thin films has been reported [22].

The aim of the present work was to delve into the formation of Ni-based mixed oxides by the reactive IBM of interfaces. To study the influence of X cation covalence in the formation of Ni-O-X mixed oxides by reactive IBM of Ni/X interfaces, the Al cation, used in a previous work [6], was replaced by Si or Cr, because the covalent character of Al-O bonds is located between those of Si-O and Cr-O bonds. The binding energy value of the O 1s core level was used to establish the covalent character of single oxides. The lower the binding energy, the higher the charge in the oxygen atom, indicating a greater charge transfer from the cation to the oxygen atom and, therefore, a less covalent bond. In this way, Ni-O-Si and Ni-O-Cr mixed oxides were formed. However, the ratio between NiO and Ni-O-X species depends on the X cation covalence, therefore suggesting the influence of chemical driving forces in the composition of the thin films formed.

2. Materials and Methods

Si(100) single crystals (n-type, 3.5 Ω·cm) manufactured by Virginia Semiconductors Inc. (Fredericksburg, VA, USA), and polycrystalline chromium sheets of 99.7% purity manufactured by Goodfellow, were used as substrates throughout this work. They were introduced into an ultrahigh vacuum system and sputter-cleaned "in situ" using a 3 keV Ar^+ beam until no impurities were detected by X-ray photoelectron spectroscopy (XPS) (SPECS, Berlin, Germany).

The Ni/Si and Ni/Cr interfaces were formed by evaporating 9 nm thick Ni layers at room temperature on Si and Cr substrates, respectively, and subsequently they were 3 keV O_2^+ ion beam mixed, as described elsewhere for the Ni/Al interface [22]. Nickel deposition was carried out in a preparation chamber attached to the analysis chamber by electron bombardment of a high purity Ni rod. The evaporation rate was determined by a quartz microbalance that could be placed in the same position that Si and Cr substrates. The pressure was always kept below 2×10^{-7} Pa during evaporation. Mg Kα radiation at a constant power of 300 W was used to acquire XPS spectra with a hemispherical analyzer (SPECS Phoibos 100 MCD-5). The binding energies were calibrated as described elsewhere [22]. The pass energy of the analyzer was set to 9 eV, giving a constant resolution of 0.9 eV.

3. Results and Discussion

Figure 1 shows the evolution of (a) Ni 2p, Si 2p and O 1s, and (b) Ni 2p, Cr 2p and O 1s core level spectra of Ni(9 nm)/Si and Ni(9 nm)/Cr interfaces, respectively, as a function of the 3 keV O_2^+ ion dose. The background of the spectra was subtracted using a modified Shirley method [23]. The Ni 2p spectra shown in Figure 1 were scaled to constant area to better observe the changes that took place with increasing the ion dose. The upper spectra, labelled as 0 ions/cm^2, are representative of metallic nickel. It should be pointed out that the $K\alpha_{3,4}$ satellite of the Ni 3s band and a minor peak of the Ni LMM Auger transition overlapped with the Si 2p and Cr 2p signals, respectively. These overlapping features can be observed in the Si 2p and Cr 2p zero ion dose spectra, respectively. In addition, the reference spectra for nickel (NiO), silicon (SiO_2) and chromium (Cr_2O_3) oxides thin films formed by 3 keV oxygen implantation up to saturation of high purity Ni, Si and Cr substrates, respectively, are also shown for comparison. The binding energies of pure nickel, Ni^0 $2p_{3/2}$ (852.7 eV), silicon, Si^0 2p (99.4 eV) and chromium, Cr^0 $2p_{3/2}$ (574.3 eV) core levels, and of the double-peaked Ni $2p_{3/2}$ main line (854, 855.5 eV), Si 2p (103.4 eV) and Cr $2p_{3/2}$ (576.3 eV) core levels of NiO, SiO_2 and Cr_2O_3 oxides, respectively, have been indicated in Figure 1 by dashed lines. Likewise, the O 1s binding energies, observed for NiO (529.3 eV), SiO_2 (532.7 eV) and Cr_2O_3 (529.8 eV) oxides have also been indicated. The NiO, SiO_2 and Cr_2O_3 reference spectra shown in Figure 1 agreed with those reported in the literature [22,24–27].

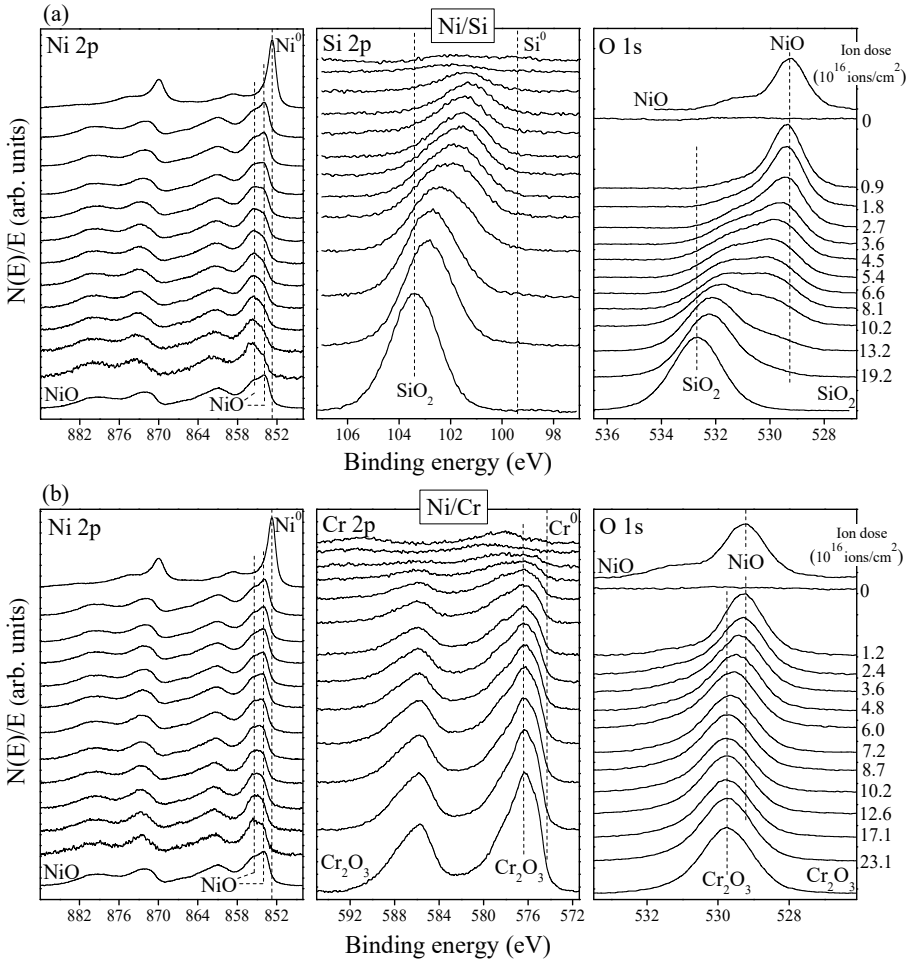

Figure 1. (**a**) Ni 2p, Si 2p and O 1s, and (**b**) Ni 2p, Cr 2p and O 1s core level spectra of the Ni(9 nm)/Si and Ni(9 nm)/Cr interfaces, respectively, as a function of the 3 keV O_2^+ ion dose. Ni 2p spectra were scaled to constant area to better observe the changes that took place with increasing the ion dose.

The changes observed in Figure 1, as the ion dose increased, were associated with the formation of Ni-O and X-O (X = Si or Cr) bonds by oxygen implantation, sputtering and intermixing of Ni and X at the interface. A fast oxidation of the deposited nickel film was observed. For an ion dose of ~1.5×10^{16} ions/cm^2, the Ni 2p core level was similar to that of NiO. Subsequently, for higher ion doses, the Ni 2p satellite structure changed and the core level shifted to higher binding energies. For the Ni/Si interface, the Si 2p core level shifted to higher binding energies as the reactive IBM proceeded, but its binding energy was always lower than that of SiO_2. Likewise, the O 1s binding energy shifted from the value observed for NiO to higher binding energies, but it was always lower than that observed for SiO_2. On the other hand, for the Ni/Cr interface, the O 1s binding energy shifted from the value observed for NiO to the value of Cr_2O_3, whereas the binding energy and shape of the Cr 2p core level remained practically constant with the increasing the ion dose, except for low ion doses when it was distorted by the overlapping with a minor peak of the Ni LMM Auger transition. The shifts and shape changes of the core levels were more pronounced for the Ni/Si than for the Ni/Cr interface. This fact could be related to the different covalent character of Si-O and Cr-O bonds. In a simple picture, assuming that final state effects may be ignored, the degree of covalence of single oxides can be related to the O 1s binding energy. The higher the O 1s binding energy, the higher the covalent character of the single oxide [28]. Therefore, SiO_2 can be considered as a strong covalent oxide, whereas Cr_2O_3 should be considered as an ionic oxide. According to this simple

picture, NiO would be a slightly more ionic oxide than Cr_2O_3, in such a way that in a Ni-O-Cr mixed oxide, the Cr-O bond would be slightly more covalent than the Ni-O bond.

The above-mentioned evolution of the core levels with increasing the ion dose suggests that Ni atoms were more ionic and Si or Cr atoms were more covalent than in single NiO and SiO_2 or Cr_2O_3 oxides, respectively. Likewise, the oxygen bonding in the Ni-O-X mixed oxides was in between the covalent character of SiO_2 or Cr_2O_3, and the ionic character of NiO [22]. According to the phenomenological rule of bonding given by Barr for mixed oxides [28], this behavior points to the formation of a Ni-O-X mixed oxide (X = Si or Cr) at higher ion doses, in good agreement with the reactive IBM of Ni/Al interfaces [22]. Moreover, the changes observed in the Ni 2p core level also support the formation of a Ni-O-X mixed oxide. This core level shifted to higher binding energy because of Ni cations increasing the ionicity in the Ni-O-X mixed oxide, as compared to that in NiO. In addition, changes in the nonlocal screening contribution to the Ni 2p core level [22,29,30] due to the presence of X cations in the oxide film were observed. The magnitude of the above-mentioned changes was more pronounced for the Ni/Si and Ni/Al [22] interfaces than for the Ni/Cr interface, therefore suggesting that they increased with the increase in the covalence of the X cation with respect to that of Ni.

Due to the high sensitivity of the Ni 2p shape core level to the Ni local environment, useful information about the evolution of the chemical composition of the thin films formed by reactive ion beam mixing can be straightforwardly obtained by the application of factor analysis (FA) to the evolution of the Ni 2p datasets of Figure 1. FA is a well-established technique to analyze a set of spectroscopic data representing the evolution of a system with respect to a parameter [22,31–34] and, in this case, with respect to the ion dose. The full mathematical details are not repeated here. The aim of FA is to reproduce the experimental dataset as a linear combination of spectra characteristic of the chemical species present in the studied system weighted by their respective concentrations. However, the number of relevant chemical species or principal factors must be determined; for example, by using the indicator function (IND) criterion [31,32]. Three principal factors were found for both interfaces, that can be attributed to Ni^0, NiO and Ni-O-X mixed oxide species, respectively, in good agreement with the behavior reported for the Ni/Al interface [22]. After Target Testing (TT) transformation [22,31–34], using Ni^0 and NiO reference spectra, and a Ni-O-X mixed oxide spectrum obtained by an iterative target testing transformation procedure [22,33,34], as target spectra, the pure component concentrations shown in Figure 2 on the left were obtained for the reactive IBM of (a) Ni/Si and (b) Ni/Cr interfaces, respectively. In addition, the target spectra used for Ni^0, NiO and Ni-O-X species are shown on the right by red dotted lines. Continuous line spectra on the right side of Figure 2a,b show the reproduction of the target spectra (red dotted lines) after TT transformation. A good agreement between the target spectra and their reproduction after TT transformation can be observed in Figure 2. This supports the validity of the predicted pure component spectra as being representative of the principal factors. A linear combination of the pure component spectra weighted by their respective concentrations perfectly reproduced the experimental data of Ni 2p in Figure 1 within the experimental error.

In good agreement with previous results for the reactive IBM of the Ni/Al interface [22], a reactive IBM kinetics of two stages was also observed for the Ni/Si and Ni/Cr interfaces. A first stage, up to ion doses of ~1.5×10^{16} ions/cm^2, characterized by the formation of NiO species, was followed by a second stage, in which the initially NiO thin film formed transformed progressively into a Ni-O-X mixed oxide, as discussed in detail for the reactive IBM of the Ni/Al interface [22]. As observed in the concentrations evolution of Figure 2, the ratio between Ni-O-X and NiO species can be tailored by varying the ion dose. It should be pointed out that the degree of transformation of NiO into Ni-O-X species depends on the covalence of the X cation. For strong covalent X cations such as Si (Figure 2a) or Al [22], NiO completely transformed into Ni-O-X species at higher ion doses, whereas for ionic cations such as Cr, the transformation was incomplete. This behavior suggests that the formation of a Ni-O-X mixed oxide is favored for X cations whose covalence is

very much higher than that of Ni, therefore suggesting that it is influenced by chemical driving forces.

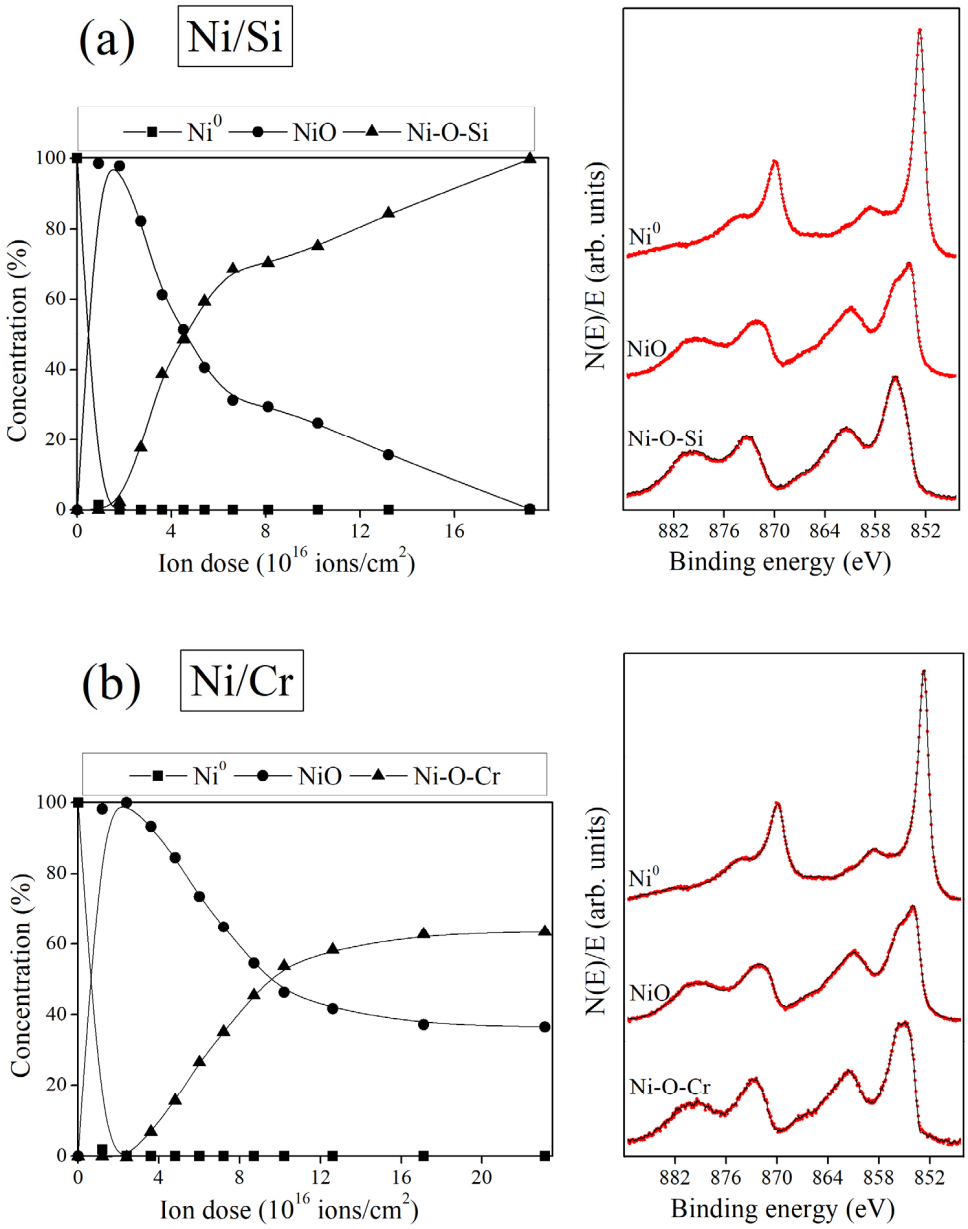

Figure 2. Ni 2p pure component concentrations, on the left, and Ni 2p target pure component spectra (red dotted lines), on the right, obtained by FA for the reactive IBM of (**a**) Ni/Si and (**b**) Ni/Cr interfaces, respectively. Continuous line spectra on the right side of (**a**) and (**b**) show the reproduction of the target spectra (red dotted lines) after Target Testing transformation.

In Figure 3, the Ni 2p pure component spectra for several Ni-O-X mixed oxide species are compared. It is worth mentioning that the single-peaked main line Ni 2p spectrum for Ni-O-Al species was found to be in good agreement with those reported for $NiAl_2O_4$ [22]. Likewise, the spectrum found for Ni-O-Cr species was similar to those reported in the literature for nickel chromite, $NiCr_2O_4$, characterized by a broad Ni $2p_{3/2}$ single-peaked main line [35]. The spectrum for the Ni-O-Si species was similar to those reported for nickel silicates, $NiSiO_3$ and Ni_2SiO_4, characterized by a Ni $2p_{3/2}$ single-peaked main line [19,36,37]. The binding energy of the single-peaked Ni $2p_{3/2}$ core level was ~855.7, 855.5 and 855.3 eV for Ni-O-Si, Ni-O-Al and Ni-O-Cr species, respectively, therefore indicating that the degree

of ionicity of Ni cations in the Ni-O-X mixed oxide increased with the increase in the covalence of the X cation, in agreement with the rule of bonding proposed by Barr for mixed oxides [12]. In addition, the characteristic double-peaked structure of the Ni $2p_{3/2}$ core level of bulk NiO disappeared in the Ni 2p spectrum of Ni-O-X species since the incorporation of X cation suppress nonlocal screening features, therefore promoting the local screening mechanism in the Ni 2p core level [22,29,30].

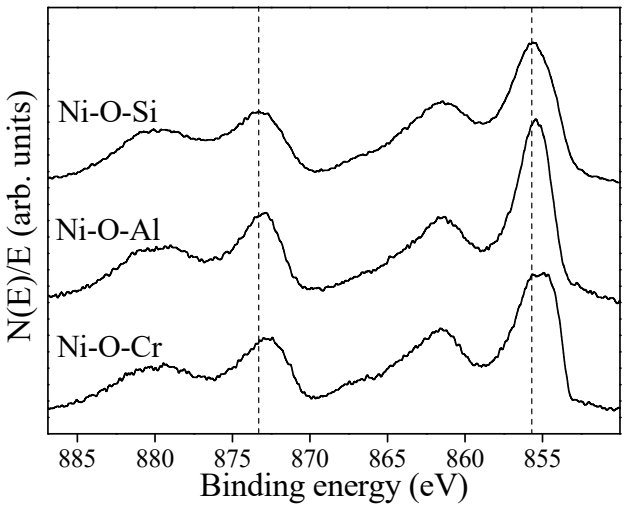

Figure 3. Ni 2p pure component spectra for several Ni-O-X mixed oxide species obtained by application of FA to the reactive IBM of Ni/X interfaces.

Information on the in-depth distribution of chemical species formed during the reactive IBM of the studied interfaces could be obtained by depth profiling. However, depth profiling of oxide films leads to preferential sputtering phenomena, in such a way that changes in the oxide stoichiometry occur by oxygen preferential sputtering [38,39]. To overcome this problem, the Ni 2p core level was measured as a function of the take-off angle, θ, to obtain, in a non-destructive way, additional qualitative information about the in-depth distribution of the different phases formed during the reactive IBM of Ni/Si and Ni/Cr interfaces. The variation of the take-off angle allowed us to change the surface sensitivity of XPS technique. From these data, the concentration of NiO and Ni-O-X species was obtained by a least-squares fitting of the Ni 2p spectra, measured as a function of the take-off angle for several ion doses, to a combination of the reproduced NiO and Ni-O-X target spectra of Figure 2. The results obtained for (a) Ni/Si and (b) Ni/Cr interfaces, respectively, are shown in Figure 4. The NiO and Ni-O-X species concentration evolution as a function of the take-off angle indicates that the film surface was enriched in Ni-O-X mixed species. This behavior was also found during the reactive IBM of Ni/Al interfaces [22]. SRIM simulations [40] allowed us to calculate a sputtering yield of 2.52, 1.29 and 2.04 atoms/ion for Ni, Si and Cr by 3 keV O_2^+ ions at normal incidence, respectively. According to these values, preferential sputtering of Ni took place, explaining the observed surface enrichment in X-containing species.

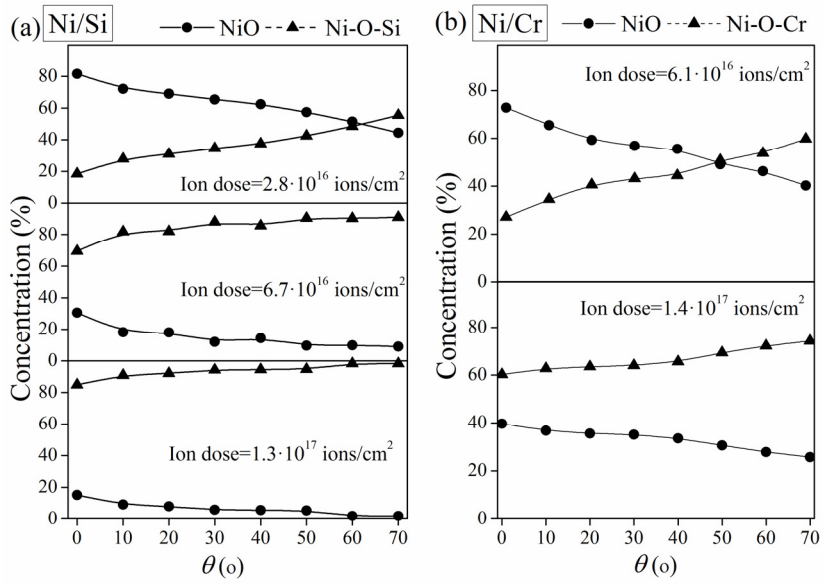

Figure 4. Concentrations of NiO and Ni-O-X species as a function of the take-off angle for (**a**) Ni/Si and (**b**) Ni/Cr interfaces, respectively, at several ion doses.

4. Conclusions

The bombardment of Ni/(Si or Cr) interfaces with O_2^+ ions at low energy (3 keV) produced the formation of Ni-O-(Si or Cr) mixed oxides. Initially, for low ion doses, only NiO was formed and that was progressively transformed into a Ni-O-(Si or Cr) mixed oxide, the degree of transformation depending on the cation covalence. For strong covalent cations (Si and Al), the transformation of Ni oxide into Ni-mixed oxide was complete for high ion doses (above 1.8×10^{17} ions/cm^2), whereas for ionic cations such as Cr, the transformation was incomplete, therefore indicating that the reaction was governed by chemical driving forces. It was observed not only that the ionicity of the Ni atoms in the Ni-mixed oxide increased with the increase in the cation covalence but also that the features appearing in the Ni 2p spectrum of bulk NiO, related to non-local screening effects, disappeared.

Author Contributions: Conceptualization, methodology, validation, formal analysis, investigation, visualization, data curation, writing—original draft preparation and writing—review and editing, A.A. and C.P. All authors have read and agreed to the published version of the manuscript.

Funding: Financial support from grant PID2020-116712RB-C21 funded by MCIN/AEI/10.13039/501100011033 is acknowledged.

Institutional Review Board Statement: Not applicable.

Informed Consent Statement: Not applicable.

Data Availability Statement: Data are contained within the article.

Acknowledgments: The authors thank Domingo Díaz for technical assistance.

Conflicts of Interest: The authors declare no conflict of interest.

References

1. Jiang, Z.; Fang, D.; Liang, Y.; He, Y.; Einaga, H.; Shangguan, W. Catalytic degradation of benzene over non-thermal plasma coupled Co-Ni binary metal oxide nanosheet catalysts. *J. Environ. Sci.* **2023**, *132*, 1–11. [CrossRef]
2. Hu, X.; Zhang, M.; Ren, A.; Huang, Y.; Yan, X.; Feng, R.; Zhao, G. Mesoporous nickel-cobalt oxide for efficient liquid-phase benzyl alcohol oxidation by air. *Catal. Today* **2022**, *405–406*, 75–81. [CrossRef]
3. Faid, A.Y.; Barnett, A.O.; Seland, F.; Sunde, S. NiCu mixed metal oxide catalyst for alkaline hydrogen evolution in anion exchange membrane water electrolysis. *Electrochim. Acta* **2021**, *371*, 137837. [CrossRef]

4. Dhas, C.R.; Monica, S.E.S.; Jothivenkatachalam, K.; Nathanael, A.J.; Kavinkumar, V.; Venkatesh, R.; Arivukarasan, D. Direct-grown nebulizer-sprayed nickel-copper mixed metal oxide nanocomposite films as bifunctional electrocatalyst for water splitting. *Ionics* **2021**, *28*, 383–396. [CrossRef]
5. Rastegarpanah, A.; Liu, Y.; Deng, J.; Jing, L.; Pei, W.; Zhang, X.; Hou, Z.; Rezaei, M.; Dai, H. Influence of preparation method on catalytic performance of three-dimensionally ordered macroporous NiO-CuO for CO oxidation. *J. Solid State Chem.* **2021**, *297*, 122091. [CrossRef]
6. Awan, I.Z.; Beltrami, G.; Bonincontro, D.; Gimello, O.; Cacciaguerra, T.; Tanchoux, N.; Martucci, A.; Albonetti, S.; Cavani, F.; Di Renzo, F. Copper-nickel mixed oxide catalysts from layered double hydroxides for the hydrogen-transfer valorisation of lignin in organosolv pulping. *Appl. Catal. A Gen.* **2021**, *609*, 117929. [CrossRef]
7. Kong, L.; Li, D.; Bi, J.; Fan, X.; Xie, Z.; Xiao, X.; Zhao, Z. Template-induced mesoporous Ni-Al oxide catalysts with tuned physico-chemical properties for the oxidative dehydrogenation of ethane. *J. Chem. Eng.* **2023**, *452*, 139247. [CrossRef]
8. Nesterov, N.S.; Pakharukova, V.P.; Philippov, A.A.; Gerasimov, E.Y.; Tsybulya, S.V.; Martyanov, O.N. Synthesis of catalytic precursors based on mixed Ni-Al oxides by supercritical antisolvent co-precipitation. *Catalysts* **2022**, *12*, 1597. [CrossRef]
9. Caravaggio, G.; Nossova, L.; Turnbull, M.J. Nickel-magnesium mixed oxide catalyst for low temperature methane oxidation. *J. Chem. Eng.* **2021**, *405*, 126862. [CrossRef]
10. Summa, P.; Gajewska, M.; Li, L.; Hu, C.; Samojeden, B.; Motak, M.; Da Costa, P. Solution combustion synthesis as an alternative synthesis route for novel Ni-Mg-Al mixed-oxide catalyst for CO_2 methanation. *J. CO_2 Util.* **2022**, *60*, 101983. [CrossRef]
11. Zahra, T.; Ahmad, K.S.; Zequine, C.; Gupta, R.; Malik, M.A.; Niazi, J.H.; Qureshi, A. Bio-inspired NiO/ZrO_2 mixed oxides (NZMO) for oxygen evolution reactions: From facile synthesis to electrochemical analysis. *J. Chem. Technol. Biotechnol.* **2023**, *98*, 296–305. [CrossRef]
12. Moschkowitsch, W.; Zion, N.; Honig, H.C.; Levy, N.; Cullen, D.A.; Elbaz, L. Mixed-Metal Nickel-Iron Oxide Aerogels for Oxygen Evolution Reaction. *ACS Catal.* **2022**, *12*, 12162–12169. [CrossRef]
13. Nozari-Asbemarz, M.; Amiri, M.; Imanzadeh, H.; Bezaatpour, A.; Nouhi, S.; Hosseini, P.; Wark, M.; Seifzadeh, D. Mixed metal oxides as efficient electrocatalysts for water oxidation. *Int. J. Hydrogen Energy* **2022**, *47*, 5250–5259. [CrossRef]
14. Devi, S.; Sunaina, R.; Wadhwa, R.; Yadav, K.K.; Jha, M. Understanding the origin of ethanol oxidation from ultrafine nickel manganese oxide nanosheets derived from spent alkaline batteries. *J. Clean. Prod.* **2022**, *376*, 134147. [CrossRef]
15. Perez, L.C.P.; Chalkley, Z.; Wendt, R.; Ahmet, I.Y.; Wollgarten, M.; Mayer, M.T. CO_2 electro reduction activity and dynamic structural evolution of in situ reduced nickel-indium mixed oxides. *J. Mat. Chem. A* **2022**, *10*, 20593–20605. [CrossRef]
16. Aberkane, A.B.; Yeste, M.P.; Djazi, F.; Cauqui, M.A. CO methanation over NiO-CeO_2 mixed-oxide catalysts prepared by a modified co-precipitation method: Effect of the preparation pH on the catalytic performance. *Nanomaterials* **2022**, *12*, 2627. [CrossRef] [PubMed]
17. Kim, D.; Surendran, S.; Lim, Y.; Choi, H.; Lim, J.; Kim, J.Y.; Han, M.; Sim, U. Spinel-type Ni_2GeO_4 electrocatalyst for electrochemical ammonia synthesis via nitrogen reduction reaction under ambient conditions. *Int. J. Energy Res.* **2021**, *46*, 4119–4129. [CrossRef]
18. Kulal, N.; Vetrivel, R.; Gopinath, C.S.; Ravindran, R.K.; Rao, V.N.; Shetty, M.; Shrikanth, R.; Rangappa, D.; Shanbhag, G.V. Green route for carbonylation of amines by CO_2 using Sn-Ni-O bifunctional catalyst and theoretical study for finding best suited active sites. *J. Eng. Chem.* **2021**, *419*, 129439. [CrossRef]
19. Zhao, Z.; Lakshminarayanan, N.; Swartz, S.L.; Arkenberg, G.B.; Felix, L.G.; Slimane, R.B.; Choi, C.C.; Ozkan, U.S. Characterization of olivine-supported nickel silicate as potential catalysts for tar removal from biomass gasification. *Appl. Cat. A Gen.* **2015**, *489*, 42–50. [CrossRef]
20. Bilal, A.; Kasi, J.K.; Kasi, A.K.; Bokhari, M.; Ahmed, S.; Ali, S.W. Environment friendly synthesis of nickel ferrite nanoparticles using Brassica oleracea var. capitate (green cabbage) as a fuel and their structural and magnetic characterizations. *Mat. Chem. Phys.* **2022**, *290*, 126483. [CrossRef]
21. Din, S.U.; Ul Haq, M.; Sajid, M.; Khatoon, R.; Chen, X.; Li, L.; Zhang, M.; Zhu, L. Development of high-performance sensor based on NiO/SnO(2)heterostructures to study sensing properties towards various reducing gases. *Nanotechnology* **2020**, *31*, 395502. [CrossRef] [PubMed]
22. Arranz, A.; Palacio, C. Nanoscale modification of Ni/Al interfaces by low-energy O_2^+ reactive ion beam mixing. *Appl. Phys. A* **2011**, *103*, 309–316. [CrossRef]
23. Proctor, A.; Sherwood, M.P.A. Data analysis techniques in x-ray photoelectron spectroscopy. *Anal. Chem.* **1982**, *54*, 13–19. [CrossRef]
24. Bell, G.G.; Ley, L. Photoemission study of SiO_x ($0 \leq x \leq 2$) alloys. *Phys. Rev. B* **1998**, *37*, 8383–8393. [CrossRef] [PubMed]
25. Guittet, M.J.; Crocombette, J.P.; Gauttier-Soyer, M. Bonding and XPS chemical shifts in $ZrSiO_4$ versus SiO_2 and ZrO_2: Charge transfer and electrostatic effects. *Phys. Rev. B* **2001**, *63*, 125117. [CrossRef]
26. Ünveren, E.; Kemnitz, E.; Hutton, S.; Lippitz, A.; Unger, W.E.S. Analysis of highly resolved x-ray photoelectron Cr 2p spectra obtained with a Cr_2O_3 powder sample prepared with adhesive tape. *Surf. Interface Anal.* **2004**, *36*, 92–95. [CrossRef]
27. Biesinger, M.C.; Brown, C.; Mycroft, J.R.; Davidson, R.D.; McIntyre, N.S. X-ray photoelectron spectroscopy studies of chromium compounds. *Surf. Interface Anal.* **2004**, *36*, 1550–1563. [CrossRef]
28. Barr, T.L. Recent advances in x-ray photoelectron spectroscopy studies of oxides. *J. Vac. Sci. Technol. A* **1991**, *9*, 1793–1805. [CrossRef]

29. Maiti, K.; Mahadevan, P.; Sarma, D.D. Evolution of electronic structure with dimensionality in divalent nickelates. *Phys. Rev. B* **1999**, *59*, 12457–12469. [CrossRef]
30. Altieri, S.; Tjeng, L.H.; Tanaka, A.; Sawatzky, G.A. Core-level x-ray photoemission on NiO in the impurity limit. *Phys Rev. B* **2000**, *61*, 13403–13409. [CrossRef]
31. Malinowski, E.R.; Howery, D.C. *Factor Analysis in Chemistry*; Krieger: Malabar, FL, USA, 1989.
32. Palacio, C.; Mathieu, H.J. Application of factor analysis to the AES and XPS study of the oxidation of chromium. *Surf. Interface Anal.* **1990**, *16*, 178–182. [CrossRef]
33. Fiedor, J.N.; Proctor, A.; Houalla, M.; Hercules, D.M. Determination of the distribution of molybdenum oxidation states in reduced Mo/TiO_2 catalysts by factor analysis and curve fitting. *Surf. Interface Anal.* **1993**, *20*, 1–9. [CrossRef]
34. Arranz, A.; Palacio, C. Composition of tantalum nitride thin films grown by low-energy nitrogen implantation: A factor analysis study of the Ta 4f XPS core level. *Appl. Phys. A* **2005**, *81*, 1405–1410. [CrossRef]
35. Lenglet, M.; d'Huysser, A.; Arsène, J.; Bonnelle, J.P.; Jørgensen, C.K. XANES, x-ray photoelectron and optical spectra of divalent nickel at the crystallographic transition in $NiCr_2O_4$ and the $Ni_{1-x}Cu_xCr_2O_4$ system: Correlation with the Jahn-Teller effect. *J. Phys. C Solid State Phys.* **1986**, *19*, L363–L368. [CrossRef]
36. Lorenz, P.; Finster, J.; Wendt, G.; Salyn, J.V.; Zumadilov, E.K.; Nefedov, V.I. Esca investigations of some NiO/SiO_2 and $NiO-Al_2O_3/SiO_2$ catalysts. *J. Electron Spectrosc. Relat. Phenom.* **1979**, *16*, 267–276. [CrossRef]
37. Shalvoy, R.B.; Reucroft, P.J.; Davis, B.H. Characterization of coprecipitated nickel on silica methanation catalysts by X-ray photoelectron spectroscopy. *J. Catal* **1979**, *56*, 336–348. [CrossRef]
38. Malherbe, J.B.; Hofmann, S.; Sanz, J.M. Preferential sputtering of oxides. A comparison of model predictions with experimental data. *Appl. Surf. Sci.* **1986**, *27*, 355–365. [CrossRef]
39. Benito, N.; Palacio, C. Nanostructuring of Ta_2O_5 surfaces by low energy Ar^+ bombardment. *Appl. Surf. Sci.* **2015**, *351*, 753–759. [CrossRef]
40. Ziegler, J.F.; Biersack, J.B.; Littmark, U. *The Stopping and Range of Ions in Matter Vol 1*; Pergamon: New York, NY, USA, 1985. Available online: https://www.SRIM.org (accessed on 4 February 2023).